Article

Synthesis of Highly Ordered Mesoporous Crystalline WS and MoS *via* a High-Temperature Reductive Sulfuration Route

Yifeng Shi, Ying Wan, Ruili Liu, Bo Tu, and Dongyuan Zhao

J. Am. Chem. Soc., **2007**, 129 (30), 9522-9531• DOI: 10.1021/ja072910n • Publication Date (Web): 11 July 2007

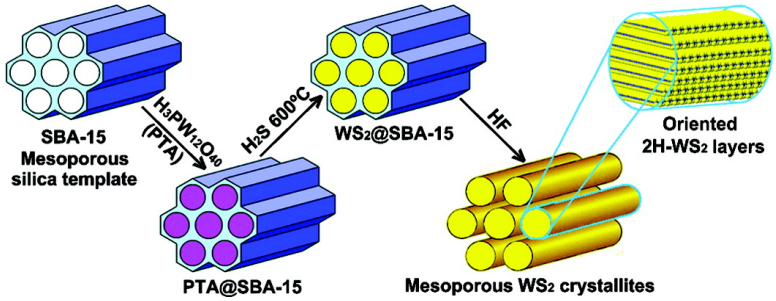

More About This Article

Additional resources and features associated with this article are available within the HTML version:

- Supporting Information
- Links to the 5 articles that cite this article, as of the time of this article download
- Access to high resolution figures
- Links to articles and content related to this article
- Copyright permission to reproduce figures and/or text from this article

View the Full Text HTML

J|A|C|S
ARTICLES
Published on Web 07/11/2007

Synthesis of Highly Ordered Mesoporous Crystalline WS_2 and MoS_2 *via* a High-Temperature Reductive Sulfuration Route

Yifeng Shi,[†] Ying Wan,[†,‡] Ruili Liu,[†] Bo Tu,[†] and Dongyuan Zhao*,[†]

Contribution from the Department of Chemistry, Shanghai Key Laboratory of Molecular Catalysis and Innovative Materials, Key Laboratory of Molecular Engineering of Polymers, Advanced Materials Laboratory, Fudan University, Shanghai 200433, P. R. China, and Department of Chemistry, Shanghai Normal University, Shanghai 200234, P. R. China

Received April 25, 2007; E-mail: dyzhao@fudan.edu.cn

Abstract: A high-temperature reductive sulfuration method is demonstrated to synthesize highly ordered mesoporous metal sulfide crystallites by using mesoporous silica as hard templates. H_2S gas is utilized as a sulfuration agent to *in situ* convert phosphotungstic acid $H_3PW_{12}O_{40}\cdot 6H_2O$ to hexagonal WS_2 crystallites in the silica nanochannels at 600 °C. Upon etching silica, mesoporous, layered WS_2 nanocrystal arrays are produced with a yield as high as 96 wt %. XRD, nitrogen sorption, SEM, and TEM results reveal that the WS_2 products replicated from the mesoporous silica SBA-15 hard template possess highly ordered hexagonal mesostructure (space group, *p*6*mm*) and rodlike morphology, analogous to the mother template. The S−W−S trilayers of the WS_2 nanocrystals are partially oriented, parallel to the mesochannels of the SBA-15 template. This orientation is related with the reduction of the high-energy layer edges in layered metal dichalcogenides and the confinement in anisotropic nanochannels. The mesostructure can be 3-D cubic bicontinuous if KIT-6 (*Ia*$\bar{3}$*d*) is used as a hard template. Mesoporous WS_2 replicas have large surface areas (105−120 m^2/g), pore volumes (∼0.20 cm^3/g), and narrow pore size distributions (∼4.8 nm). By one-step nanocasting with the $H_3PMo_{12}O_{40}\cdot 6H_2O$ (PMA) precursor into the mesochannels of SBA-15 or KIT-6 hard template, highly ordered mesoporous MoS_2 layered crystallites with the 2-D hexagonal (*p*6*mm*) and 3-D bicontinuous cubic (*Ia*$\bar{3}$*d*) structures can also be prepared *via* this high-temperature reductive sulfuration route. When the loading amount of PMA precursor is low, multiwalled MoS_2 nanotubes with 5−7 nm in diameter can be obtained. The high-temperature reductive sulfuration method is a general strategy and can be extended to synthesize mesoporous CdS crystals and other metal sulfides.

Introduction

Metal chalcogenides exhibit technically useful, unique optical and electronic properties, which inspire the fabrication of their nanocrystals, nanotubes, and nanorods.[1−4] Among them, an attractive vision is transition metal dichalcogenide MX_2 (M = Mo, W, Ti, Zr, Hf, V, Nb, and Ta, X = S, Se) which constitutes a layered structure in analogy to graphite.[5−9] The layered structure is constructed by unit X−M−X atomic trilayers which are connected by strongly covalent bonding and lattice layers. The latter is formed by the weak van der Waals attraction.[5−7] It is the large band-edge excitation of the metal centered *d*−*d* transition that gives rise to the unique electronic features and, therefore, results in numerous applications in hydrodesulfurization catalysis,[10−12] electrochemical intercalation,[13,14] solid lubrication,[15,16] hydrogen storage,[17,18] elastic and coating materials,[19,20] and Li batteries.[21,22] Nanosized arrays of these materials with ordered mesostructures and high surface areas may provide quantum confinement and enhance their properties in the demand for high-tech and advanced materials.[23,24] However, it is a great challenge to synthesize ordered nanoporous metal sulfides due to the uncontrollable fast precipitation between metal ions and the S^{2-} ion.[25,26]

† Fudan University.
‡ Shanghai Normal University.

(1) Chianelli, R. R.; Berhault, G.; Santiago, P.; Mendoza, D.; Espinosa, A.; Ascencio, J. A.; Yacaman, M. J. *Mater. Technol.* **2000**, *15*, 54.
(2) Bochmann, M. *Chem. Vap. Deposition* **1996**, *2*, 85.
(3) Mitchell, K.; Ibers, J. A. *Chem. Rev.* **2002**, *102*, 1929.
(4) Hautala, J.; Taylor, P. C. *J. Non-Cryst. Solids* **1992**, *141*, 24.
(5) Remskar, M. *Adv. Mater.* **2004**, *16*, 1497.
(6) Rao, C. N. R.; Nath, M. *Dalton Trans.* **2003**, 1.
(7) Tremel, W. *Angew. Chem., Int. Ed.* **1999**, *38*, 2175.
(8) Tenne, R. *Nat. Nanotechnol.* **2006**, *1*, 103.
(9) Tenne, R. *Angew. Chem., Int. Ed.* **2003**, *42*, 5124.
(10) Skrabalak, S. E.; Suslick, K. S. *J. Am. Chem. Soc.* **2005**, *127*, 9990.
(11) Byskov, L. S.; Norskov, J. K.; Clausen, B. S.; Topsoe, H. *J. Catal.* **1999**, *187*, 109.
(12) Daage, M.; Chianelli, R. R. *J. Catal.* **1994**, *149*, 414.
(13) Li, L.; Li, Y. D. *J. Phys. Chem. B* **2004**, *108*, 13893.
(14) Homyonfer, M.; Alperson, B.; Rosenberg, Y.; Sapir, L.; Cohen, S. R.; Hodes, G.; Tenne, R. *J. Am. Chem. Soc.* **1997**, *119*, 2693.
(15) Rapoport, L.; Fleischer, N.; Tenne, R. *J. Mater. Chem.* **2005**, *15*, 1782.
(16) Rapoport, L.; Bilik, Y.; Feldman, Y.; Homyonfer, M.; Cohen, S. R.; Tenne, R. *Nature* **1997**, *387*, 791.
(17) Chen, J.; Li, S. L.; Tao, Z. L.; Shen, Y. T.; Cui, C. X. *J. Am. Chem. Soc.* **2003**, *125*, 5284.
(18) Chen, J.; Kuriyama, N.; Yuan, H.; Takeshita, H. T.; Sakai, T. *J. Am. Chem. Soc.* **2001**, *123*, 11813.
(19) Singer, L.; Fayeulle, S.; Ehni, P. D. *Wear* **1996**, *195*, 7.
(20) Singer, L.; Bolster, R. N.; Wegand, J.; Fayeulle, S.; Stupp, B. C. *Appl. Phys. Lett.* **1990**, *57*, 995.
(21) Miki, Y.; Nakazato, D.; Ikuta, H.; Uchida, T.; Wakihara, M. *J. Power Sources* **1995**, *54*, 508.
(22) Julien, C.; Saikh, S. I.; Nazri, G. A. *Mater. Sci. Eng. B* **1992**, *15*, 73.
(23) Turner, E. A.; Huang, Y. N.; Corrigan, J. F. *Eur. J. Inorg. Chem.* **2005**, 4465.
(24) Thiruvengadathan, R.; Regev, O. *Chem. Mater.* **2005**, *17*, 3281.
(25) Li, H.; Zhao, X. P.; Yan, C. M. *Mater. Lett.* **2006**, *60*, 2896.

 10.1021/ja072910n CCC: $37.00

A surfactant templating approach, reported by Braun et al., can be considered as the first effort to prepare ordered two-dimensional (2-D) hexagonal (*p*6*mm*) or lamellar mesostructured CdS, ZnS, and $CdZnS_2$ materials by using oligoethylene oxide oleyl ether as a structure-directing agent (SDA).[27−30] Lubeck et al. developed this method to prepare mesostructured CuS by utilizing the cationic exchange of Cu^{2+} with intermediate mesostructured CdS.[31] Mesostructured metal chalcogenides can also be obtained by supermolecular assembly of Zintl anions with transition metals, such as $[MQ_4]^{4-}$, $[M_2Q_6]^{4-}$, $[M_4Q_{10}]^{4-}$ (M = Sn, Sb, Ge, Mo; Q = S, Se, Te),[32−35] or metal carbonyls, like $W(CO)_6$ and $Mo(CO)_6$.[36] Unfortunately, the demand of strong interaction between inorganic precursors and organic SDAs limits the compositions in the assembly. However, for all these reported metal chalcogenides materials, highly ordered mesostructures could not be retained after the removal of surfactant templates either by calcination or by solvent extraction. The ordered mesopores have not been rendered.

The hard templating route has also been explored to fabricate ordered metal sulfide replicas by using mesoporous silica as a hard template. Utilizing the $[Cd_{10}S_{16}C_{32}H_{80}N_4O_{28}]$ cluster as a precursor, Gao et al. fabricated ordered 2-D hexagonal mesoporous CdS nanowire arrays.[37] The precursor contains both Cd and S and can be thermally decomposed to CdS at 160 °C in air. The usage of this special cluster makes it unfeasible to other compositions. In addition, the mesotunnels in the walls of the silica template are important. These mesotunnels generate interconnected nanopillars which support the final replicas. Liu et al. nanocasted a mixture of thiourea and metal nitrates into mesoporous silica channels to prepare mesoporous CdS, ZnS, and In_2S_3 with nanoparticle pore walls and the 2-D hexagonal structure.[38] Thiourea serves as a sulfide source that can slow down the formation rate of metal sulfides. However, two individual precursors were involved in the impregnation step. This led to a low loading amount as well as a large weight loss and, in turn, a low yield (37.6 wt %). The method is restricted to the above-mentioned materials due to the low decomposition temperature of thiourea (∼150 °C). A lot of metal precursors such as $H_3PW_{12}O_{40}\cdot 6H_2O$ (PTA) and $H_3PMo_{12}O_{40}\cdot 6H_2O$ (PMA) cannot be sulfurated at such a low reaction temperature.

Here we demonstrate a novel high-temperature reductive sulfuration approach to fabricate highly ordered mesoporous crystalline WS_2 and MoS_2. Ordered mesoporous silicas are used as hard templates. The metal precursors are phosphotungstic acid (PTA) and phosphomolybdic acid (PMA), which can be easily nanocasted into the silica nanochannels in one step. The metal precursors (PTA and PMA)/silica composites can be converted to hexagonal WS_2 and MoS_2 crystallites by using H_2S gas as a sulfuration agent at a high temperature of 600 °C. After etching the silica template, highly ordered 2-D hexagonal (*p*6*mm*) and 3-D bicontinuous cubic ($Ia\bar{3}d$) mesostructured WS_2 and MoS_2 nanocrystal arrays can be successfully obtained with a high yield (WS_2: 96 wt % and MoS_2: 97 wt %). The mesostructure and morphology as well as the compositions of the metal sulfides can be tuned by the adjustment of the mother template, the loading amount of the precursor, and the metal precursor. Mesoporous WS_2 and MoS_2 replicas have large surface areas (96−120 m^2/g), pore volumes (0.15−0.21 cm^3/g), and narrow pore size distributions (4.6−5.0 nm). Layered WS_2 and MoS_2 nanocrystals are partially oriented along the mesochannels of the silica templates. The confined growth inside the mesochannels can also generate multiwalled MoS_2 nanotubes with diameters of 5−7 nm in the case of a low loading amount of the metal precursor. This high-temperature reductive sulfuration method is a general strategy and can be extended to synthesize mesoporous metal sulfides such as CdS.

Experimental Section

Chemicals. Triblock poly(ethylene oxide)-*b*-poly(propylene oxide)-*b*-poly(ethylene oxide) copolymer Pluronic P123 (M_w = 5800, EO_{20}-$PO_{70}EO_{20}$) was purchased from Aldrich Chemical Inc. Phosphotungstic acid $H_3PW_{12}O_{40}\cdot xH_2O$ (PTA, AR), phosphomolybdic acid $H_3PMo_{12}O_{40}\cdot xH_2O$ (PMA, AR), sublimed sulfur powder (purity >99.5%), and hydrogen gas (purity >99.99%) were purchased from Sinopharm Chemical Reagent Co., Ltd. The raw PTA and PMA reagents were purified by recrystallization in ethanol before use, and the $H_3PW_{12}O_{40}\cdot 6H_2O$ and $H_3PMo_{12}O_{40}\cdot 6H_2O$ crystals were obtained and used as the precursors. All other chemicals were used as received without any further purification.

Synthesis. Mesoporous silica SBA-15[39,40] and KIT-6[41] hard templates were prepared under hydrothermal conditions of 130 °C for 24 h, according to the established procedures. Highly ordered mesoporous tungsten disulfide WS_2 materials were prepared *via* a high-temperature (600 °C) reductive sulfuration method. The first step was a nanocasting process. The PTA precursor was incorporated into the channels of mesoporous silica *via* a solvent evaporation induced impregnation process.[42,43] The subsequent high-temperature reductive sulfuration was carried out in an apparatus as shown in Figure S1 in the Supporting Information. The nanocasted PTA/silica composites were put inside an airproof furnace and *in situ* sulfurated by H_2S in H_2 gas at a high temperature (600 °C). The tube furnace was connected by a three-neck bottle with sulfur powders and a collector with a 2 M sodium hydroxide solution. Hydrogen sulfide gas was produced from the reaction between the hydrogen flow and the liquid sulfur in the three-neck bottle. Finally, the mesoporous silica hard template was etched by HF solution. [**WARNING**: *H_2S is a toxic gas. All these manipulations must be carried on in a ventilating cabinet for safety, and the entire gas line must be cleaned before each synthesis.*]

For a typical procedure, 1.00 g of SBA-15 template and 4.27 g of purified PTA powders were added into an open crucible with 20.0 g

(26) Zhang, Q. M.; Li, Y.; Huang, F. H.; Gu, Z. N. *J. Mater. Sci. Lett.* **2001**, *20*, 1233.
(27) Braun, P. V.; Osenar, P.; Stupp, S. I. *Nature* **1996**, *380*, 325.
(28) Braun, P. V.; Osenar, P.; Tohver, V.; Kennedy, S. B.; Stupp, S. I. *J. Am. Chem. Soc.* **1999**, *121*, 7302.
(29) Braun, P. V.; Stupp, S. I. *Mater. Res. Bull.* **1999**, *34*, 463.
(30) Tohver, V.; Braun, P. V.; Pralle, M. U.; Stupp, S. I. *Chem. Mater.* **1997**, *9*, 1495.
(31) Lubeck, C. R.; Han, T. Y. J.; Gash, A. E.; Satcher, J. H.; Doyle, F. M. *Adv. Mater.* **2006**, *18*, 781.
(32) Trikalitis, P. N.; Rangan, K. K.; Kanatzidis, M. G. *J. Am. Chem. Soc.* **2002**, *124*, 2604.
(33) Rangan, K. K.; Trikalitis, P. N.; Bakas, T.; Kanatzidis, M. G. *Chem. Commun.* **2001**, 809.
(34) Trikalitis, P. N.; Rangan, K. K.; Bakas, T.; Kanatzidis, M. G. *Nature* **2001**, *410*, 671.
(35) Wachhold, M.; Rangan, K. K.; Lei, M.; Thorpe, M. F.; Billinge, S. J. L.; Petkov, V.; Heising, J.; Kanatzidis, M. G. *J. Solid State Chem.* **2000**, *152*, 21.
(36) Vanchura, B. A.; He, P. G.; Antochshuk, V.; Jaroniec, M.; Ferryman, A.; Barbash, D.; Fulghum, J. E.; Huang, S. P. *J. Am. Chem. Soc.* **2002**, *124*, 12090.
(37) Gao, F.; Lu, Q. Y.; Zhao, D. Y. *Adv. Mater.* **2003**, *15*, 739.
(38) Liu, X. Y.; Tian, B. Z.; Yu, C. Z.; Tu, B.; Liu, Z.; Terasaki, O.; Zhao, D. Y. *Chem. Lett.* **2003**, *32*, 824.
(39) Zhao, D. Y.; Feng, J. L.; Huo, Q. S.; Melosh, N.; Fredrickson, G. H.; Chmelka, B. F.; Stucky, G. D. *Science* **1998**, *279*, 548.
(40) Zhao, D. Y.; Huo, Q. S.; Feng, J. L.; Chmelka, B. F.; Stucky, G. D. *J. Am. Chem. Soc.* **1998**, *120*, 6024.
(41) Kleitz, F.; Choi, S. H.; Ryoo, R. *Chem. Commun.* **2003**, 2136.
(42) Jiao, F.; Harrison, A.; Jumas, J. C.; Chadwick, A. V.; Kockelmann, W.; Bruce, P. G. *J. Am. Chem. Soc.* **2006**, *128*, 5468.
(43) Tian, B. Z.; Liu, X. Y.; Yang, H. F.; Xie, S. H.; Yu, C. Z.; Tu, B.; Zhao, D. Y. *Adv. Mater.* **2003**, *15*, 1370.

of ethanol. The mixture was stirred at room temperature (20−30 °C) until ethanol was evaporated. The residual powders (~5.3 g) were dried at 60 °C for 12 h to obtain PTA/mesoporous silica nanocomposites (denoted as PTA@SBA-15) and then transferred into a tube furnace for sulfuration. The whole system including the furnace and the three-neck bottle with sulfur was airproofed and swept by hydrogen to completely remove air. Then sulfur powders were heated to 380 °C, and the hydrogen gas flow was fixed at a rate of 500 mL/min. H_2S gas could be on-line produced with a volume content of about 0.6 v%. After 30 min, the furnace was heated to 600 °C at a rate of 1 °C/min and kept at this temperature for 5 h. When the furnace was cooled down to a temperature below 200 °C, the heating mantle was turned off to stop feeding the H_2S gas. Dark brown powders WS_2@SBA-15 (5.20 g) were collected after the furnace was cooled down to room temperature. The obtained powders were stirred with 60 mL of 4 wt % HF aqueous solution for 2 h to etch silica. 4.10 g of final mesoporous WS_2 products (named as WS_2-SBA-15) were collected by washing with water and acetone, filtering, and drying at 80 °C for 12 h. The final yield was 96 wt % on the basis of PTA.

Ordered mesoporous MoS_2 samples were prepared in a similar procedure by replacing PTA with PMA (3.85 g PMA per 1.00 g KIT-6). The yield was 97 wt % on the basis of PMA. Under the similar procedure, ordered mesoporous CdS replicas were prepared by using $Cd(NO_3)_2{\cdot}4H_2O$ as a precursor *via* the reductive sulfuration by H_2S at 300−400 °C.

Characterization. Powder X-ray diffraction (XRD) patterns were recorded by a D4 Endeavor powder X-ray diffractometer (Bruker, Germany) with Ni-filtered Cu Kα radiation (40 kV, 40 mA). Nitrogen adsorption−desorption isotherms were measured at −196 °C on a Micromeritics Tristars 3000 analyzer (USA). Before the measurements, the samples were outgassed at 160 °C in a vacuum for 6 h. The Brumauer−Emmett−Teller (BET) method was utilized to calculate the specific surface areas by using adsorption data in a relative pressure range from 0.02 to 0.30. The pore-size distributions (PSD) were derived from the adsorption branches of the isotherms by using the Barrett−Joyner−Halenda (BJH) method. The total pore volumes, V_p, were estimated from the adsorbed amount at a relative pressure of $p/p_0 = 0.99$. Transmission electron microscopy (TEM) experiments were conducted on a JEOL 2011 microscope operated at 200 kV. The samples were first dispersed in ethanol and then collected using copper grids covered with carbon films for analysis. Energy dispersive X-ray spectroscopy (EDX) was performed on a Philips EDAX instrument. Scanning electron microscopy (SEM) images were taken with a Philips XL30 electron microscope operating at 20 kV. A thin gold film was sprayed on the sample before this characterization. The elemental analysis for tungsten content was determined using an S4 Explorer wavelength dispersive X-ray fluorescence spectrometer (Bruker-AXS).

Results and Discussion

The mesoporous silica SBA-15 hard templates were synthesized at a high hydrothermal temperature of 130 °C to increase the mesotunnels in the wall of the mesoporous silica template, which are beneficial for the production of high-quality replica materials. The small-angle XRD pattern of this material shows five well-resolved diffraction peaks (Figure 1a), which are indexed to 100, 110, 200, 210, and 220 Bragg reflections of the hexagonal *p*6*mm* symmetry. It indicates a highly ordered mesostructure with a cell parameter (a_0) of 11.3 nm (Table 1). Upon nanocasting, the PTA/silica nanocomposite (PTA@SBA-15) displays a one-peak diffraction pattern. The cell parameter is 11.2 nm, close to that of mother template SBA-15. It implies that the mesostructure is retained after the impregnation of PTA into the mesochannels of the SBA-15 template. The tremendous decrease of the diffraction intensity for the nanocomposite

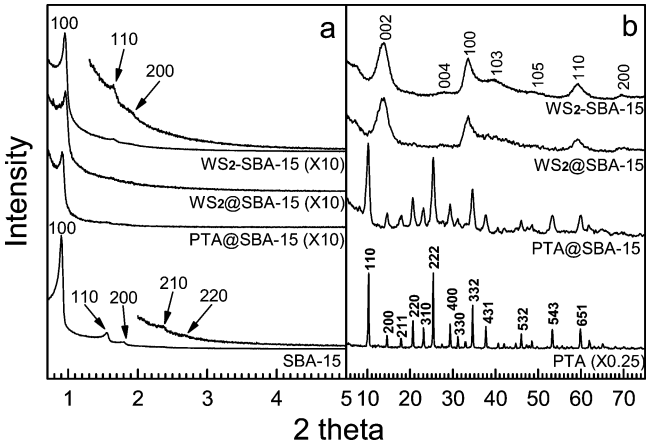

Figure 1. Powder small-angle XRD (a) and wide-angle XRD (b) patterns of the mesoporous silica SBA-15 hard template, the PTA precursor, the mesostructured PTA@SBA-15 composite prepared by impregnating PTA into the SBA-15 mesochannels, the mesostructured WS_2@SBA-15 prepared *via* the high-temperature reductive sulfuration of PTA@SBA-15 with H_2S gas at 600 °C, and the mesoporous WS_2-SBA-15 products after the removal of silica by HF etching.

Table 1. Textural Properties of Mesostructured Products

sample name	*d* (nm)	cell parameter (nm)	BET surface area (m^2/g)	pore size (nm)	pore volume (cm^3/g)
SBA-15	9.80	11.3	587	9.9	1.22
PTA@SBA-15	9.75	11.2	48	9.5	0.05
WS_2@SBA-15	9.24	10.7	34	9.3	0.03
WS_2-SBA-15	9.29	10.7	105	4.8	0.21
MoS_2-SBA-15	9.31	10.8	96	4.6	0.18
CdS-SBA-15	9.45	10.9	85	5−20	0.31
KIT-6	9.28	22.8	673	9.7	1.10
WS_2-KIT-6	8.69	21.3	120	5.0	0.17
MoS_2-KIT-6	8.87	21.7	101	4.7	0.15
CdS−KIT-6	8.90	21.8	78	5−20	0.29

PTA@SBA-15 is probably due to the reduction of the contrast and the strong X-ray absorption from heavy tungsten atoms. The XRD pattern for the nanocomposite treated by H_2S reductive sulfuration at 600 °C shows one weak diffraction peak, similar to that of PTA/silica. A shift of the diffraction peak to high 2θ value is clearly observed, indicating a shrinkage (5.3%) of the domain size upon the high-temperature treatment. After etching the silica scaffold with HF aqueous solution, the WS_2 products exhibit three resolved diffraction peaks, assigned to 100, 110, and 200 reflections of a highly ordered 2-D hexagonal mesostructure. It indicates that WS_2 crystal nanoarrays well replicate the ordered mesostructure of the SBA-15 template. The cell parameter (a_0) is calculated to be 10.7 nm. By comparing this value with that of the SBA-15 template, the structural shrinkage is estimated to be 5.3%, suggesting that the template-removal process does not cause any further shrinkage in domain size.

The crystal-phase transformation during the entire synthesis process was monitored by wide-angle XRD patterns (Figure 1b). Before the one-step nanocasting, the PTA precursors were recrystallized. All diffraction peaks of the purified PTA precursors can be indexed to a pure $H_3PW_{12}O_{40}{\cdot}6H_2O$ phase (JCPDS: 50-0304) without any detectable impurity. After the solvent evaporation induced impregnation process in mesoporous silica SBA-15, the positions of the diffraction peaks remain the same,

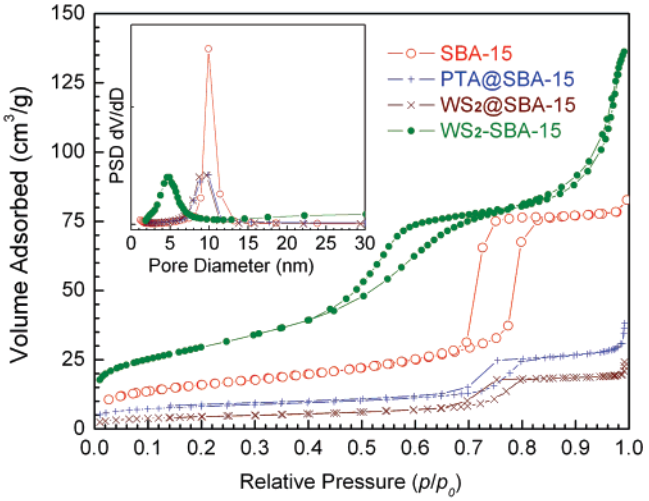

Figure 2. Nitrogen sorption isotherms of the samples successively produced in the synthesis: the SBA-15 hard template (○), PTA@SBA-15 composites (+) prepared by the impregnation of PTA into SBA-15, WS_2@SBA-15 (×) obtained from the high-temperature reductive sulfuration with H_2S gas at 600 °C, and WS_2-SBA-15 replicas (●) etched by HF solution. Inset is corresponding pore-size distribution curves. The adsorbed amount of SBA-15 was reduced by 10 times for clarity.

but the intensities become comparatively weak and the width gets wide. These phenomena imply that the PTA precursors have been incorporated into the nanochannels of the SBA-15 template with the maintenance of the crystal phase. Compared to the bulk sample, the crystal sizes are smaller owing to the confined growth inside the mesochannels. The subsequent reductive sulfuration treatment at 600 °C under H_2S in H_2 gas leads to a totally different XRD pattern. Seven broad diffractions can be observed, which can be indexed to 002, 004, 100, 103, 105, 110, and 200 reflections from the hexagonal (space group of $P6_3/mmc$) 2H-WS_2 structure (JCPDS: 84-1398; 2H means that the crystal system is **H**exagonal and one crystal cell contains two sheets of the S−W−S layer). These results suggest the formation of nanosized WS_2 in the nanochannels. No other diffraction peaks that belong to PTA, W, WO_3, and WO_2 are found, suggesting a complete transformation of PTA to WS_2. The XRD pattern almost remains unchanged upon etching silica with 4 wt % HF aqueous solution, indicating the good stability of WS_2. The elemental analysis further reveals that the final products contain about 75.3 wt % W. This value is close to the theoretical content (74.14 wt %) in the stoichiometric tungsten disulfide, implying the formation of pure WS_2 crystallites.

Figure 2 shows the nitrogen sorption isotherms of the materials successively obtained in the synthesis process. The isotherms of the SBA-15 template show typical type-IV curves with an H_1-type hysteresis loop, attributed to perfect cylindrical mesopore channels (Figure 2). The pore volume is 1.22 cm^3/g. The adsorption volume for the PTA@SBA-15 nanocomposite is 0.05 cm^3/g, suppressed by 24 times after the one-step nanocasting process. Upon the high-temperature reductive sulfuration, the WS_2@SBA-15 nanocomposite exhibits a pore volume of 0.03 cm^3/g, implying a high volume conversion from PTA to WS_2. Mesoporous WS_2 products after etching silica template show type-IV isotherms with a distinct condensation step at a p/p_0 range of 0.5−0.7, suggesting uniform mesopores (~4.8 nm). The isotherms are similar to those for highly ordered mesoporous carbons replicated from SBA-15.[44] The mesopore size of the replicas reflects the pore wall thickness of the hard template. A rapid increase in the adsorption at the p/p_0 range 0.9−1.0 is detected. It implies the presence of some voids (textual porosity), due to the incomplete filling of WS_2 inside SBA-15 pores. This phenomenon may be caused by the volume loss from PTA to WS_2 (about 30% in theory). In addition, the pores in the SBA-15 template could not be fully utilized by PTA molecules. The diameter of PTA molecules is about 1 nm, which cannot reach the micropores of SBA-15 smaller than 1 nm. On the other hand, the large PTA molecules cannot fill all the spaces in the mesopores and generate voids themselves unlike nitrogen with a small molecular size. Theoretically, about 8.0 g of WS_2 can be filled into all the mesochannels of 1.0 g of the SBA-15 template according to the calculation based on the original pore volume (1.22 cm^3/g), structure shrinkage (5.3%), and density of WS_2 (7.76 g/cm^3). In our case, about 4.1 g of WS_2 were incorporated in 1.0 g of SBA-15, which was obviously lower than the theoretical value. This estimation implies that some void spaces generated were responsible for these large pores. SEM images also give some evidence for the existence of the large pores: the surface of the product particles is not as smooth as their mother template, and lots of ravines can be found. The BET surface area of mesoporous WS_2 products is 105 m^2/g, the largest one among the reported pure WS_2 materials. In consideration of the high density of WS_2 (7.76 g/cm^3), this value is comparable to about 450 m^2/g for mesoporous silica, further demonstrating high-quality mesoporous WS_2 replicas.

The representative TEM images (Figure 3a) reveal that the mesoporous WS_2 products have a rodlike morphology with particle diameters of about 0.6−0.8 μm, analogous to the mother SBA-15 template. These phenomena may reflect a perfect duplication of the hard template and a high yield for the incorporation of WS_2 (see below detail discussion). High magnification TEM images (Figure 3b) show that these particles are constructed by aligned nanowires in whole domains. It confirms that the WS_2 replicas have a highly ordered 2-D hexagonal mesostructure. The cell parameter (a_0) estimated from the TEM images is approximately 10.5 nm, in good agreement with the value calculated from the XRD data. High-resolution TEM (HRTEM) images (Figure 3c and f) show that these nanowires are constituted by nanosized crystallized WS_2 with a layered structure. The interlayer distance is about 0.64 nm, in accordance with the d_{002}-spacing estimated from the wide-angle XRD patterns. This value is slightly larger than that (0.616 nm) previously reported from bulk WS_2 powders (JCPDS: 84-1398), which can be attributed to the twisted and nanosized WS_2 crystal structure. The EDX spectrum of the nanowire arrays displays strong signals from W and S elements without the detection of silicon, phosphorus, and oxygen elements (Figure 3g). It indicates the complete transformation of PTA and elimination of silica. That phosphorus is undetectable may be attributed to the formation and the release of gaseous P_xS_y during the high-temperature sulfuration.[45,46] At least five diffraction rings can be observed in the selected-area electron diffraction (SAED)

(44) Jun, S.; Joo, S. H.; Ryoo, R.; Kruk, M.; Jaroniec, M.; Liu, Z.; Ohsuna, T.; Terasaki, O. *J. Am. Chem. Soc.* **2000**, *122*, 10712.
(45) Jason, M. E. *Inorg. Chem.* **1997**, *36*, 2641.
(46) Keck, H.; Kuchen, W.; Renneberg, H.; Terlouw, J. K.; Visser, H. C. *Chem. Ber.* **1989**, *122*, 2265.

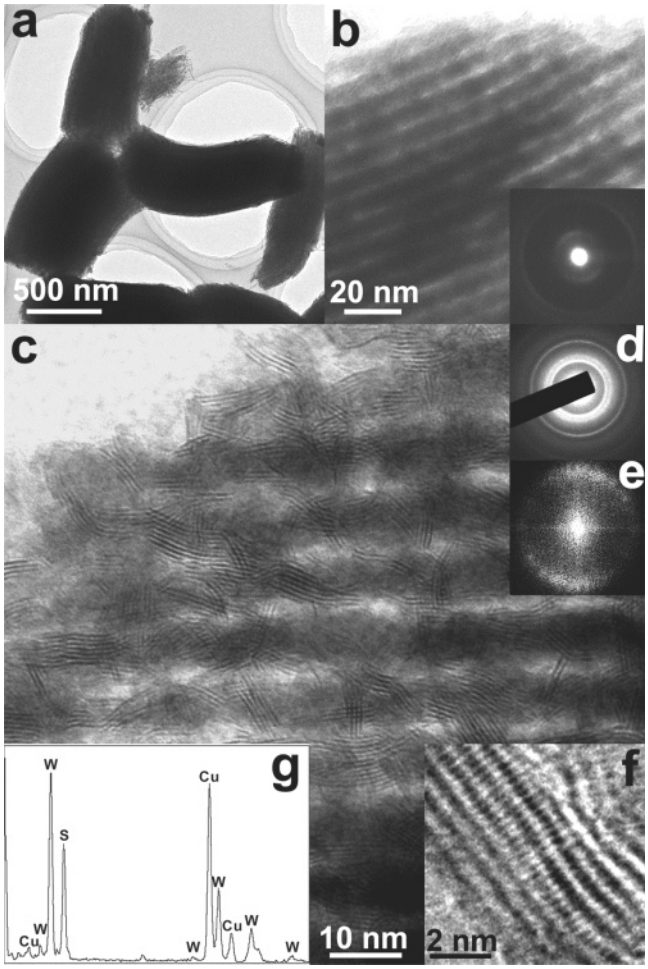

Figure 3. TEM images and EDX spectrum of mesoporous WS_2-SBA-15 replicas prepared via high-temperature reductive sulfuration method with H_2S gas at 600 °C: (a) low-magnification TEM image; (b) high-magnification TEM image; (c) and (f) HRTEM images; inset (b) and (d) are the corresponding SAED patterns of (b); (e) the corresponding FFT diffractogram of (c); and (g) EDX spectrum.

pattern (Figure 3d) taken from the area as shown in Figure 3b, caused by the nanosized crystals. The interplanar distances calculated from the diffraction rings accurately match the *d*-spacing values measured from the XRD patterns. These results confirm that the nanoarrays are composed of layered, crystallized 2H-WS_2.

It is worth noting that the orientation of WS_2 is not entirely random. The SAED measurement shows that the diffraction intensity is nonuniform in direction (Figure 3b inset), suggesting that the layered WS_2 nanocrystals are indeed partially oriented. The clear crescent pattern for the 002 diffraction further suggests that most WS_2 layers are parallel to the long axis of the nanowires replicated from the cylindrical mesochannels of SBA-15. This correlation in tropism can be directly revealed from the HRTEM images (Figure 3c) and further confirmed by the corresponding Fourier diffractogram (Figure 3e). Some nanocrystalline WS_2 layers are apparently slanted to the nanowires. It is because WS_2 nanocrystals in one nanowire can perforate the mesotunnels of SBA-15 to arrive at another one. Like a vine, the growth of layered nanocrystals is along the nanospace, both cylindrical mesochannels and mesotunnels which are slanted to the former. A switching orientation is the result when coming across mesotunnels (Figure 3c). A set of TEM images

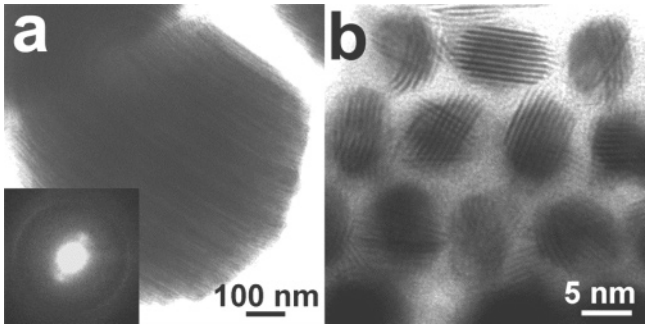

Figure 4. TEM (a) and HRTEM (b) images of mesostructured WS_2@SBA-15 nanocomposites replicated from mesoporous silica 70-SBA-15 prepared by hydrothermal treatment at 70 °C. Inset is the corresponding SAED pattern.

(no shown here) taken by the tilted technology further confirm it. These results imply the confined growth of WS_2 nanocrystals. The orientation is dependent on the main mesochannels and can be influenced by the mesotunnels in the pore walls of the SBA-15 template.

To give further evidence for the orientation of WS_2 crystallites in the confined mesochannels, the SBA-15 template with small secondary mesotunnels was synthesized according to the established low-temperature hydrothermal treatment. The ordered mesoporous silica SBA-15 which was prepared at 70 °C (denoted as 70-SBA-15, SI Figure S2) was used as a hard template to cast WS_2@70-SBA-15 nanocomposites. This hard template has a lower degree of tunnel connectivity than the regular materials. The TEM image (Figure 4a) shows that the WS_2-filled mesochannels are parallel to each other from top-left to bottom-right, indicative of a being fully filled. Only two spots corresponding to the 002 diffraction are found in the corresponding SAED pattern (Figure 4a inset), instead of two crescent diffractions observed previously. This phenomenon demonstrates that almost all WS_2 crystal layers are parallel to the long axis of the hexagonal mesostructure. The HRTEM images taken from the [001] direction are shown in Figure 4b. The typical layered structure with a spacing interval of 0.64 nm can be clearly observed in each mesopore, further suggesting that all WS_2 crystal layers are parallel to the cylindrical mesopores. Unfortunately, the mesoscale arrangement collapsed when the silica was etched from the WS_2@70-SBA-15 nanocomposite. WS_2 nanocrystals with lengths more than 100 nm were the products. It is due to the absence of enough connections between these nanowires.[47−50]

The relationship between the orientation of the guest nanowire crystals replicated by the nanocasting strategy and the mesochannels of the host is of great significance for quantum effects and applications in nanodevices. However, most nanocasted mesoporous metals and metal oxides replicas were constructed by randomly orientated crystallites.[43,51] The critical correlation could not be established, possibly due to the mismatch between the symmetries as well as the huge difference in the periodic

(47) Rumplecker, A.; Kleitz, F.; Salabas, E. L.; Schuth, F. *Chem. Mater.* **2007**, *19*, 485.
(48) Salabas, E. L.; Rumplecker, A.; Kleitz, F.; Radu, F.; Schuth, F. *Nano Lett.* **2006**, *6*, 2977.
(49) Sayari, A.; Yang, Y. *Chem. Mater.* **2005**, *17*, 6108.
(50) Yu, C. Z.; Fan, J.; Tian, B. Z.; Zhao, D. Y.; Stucky, G. D. *Adv. Mater.* **2002**, *14*, 1742.
(51) Tian, B. Z.; Liu, X. Y.; Solovyov, L. A.; Liu, Z.; Yang, H. F.; Zhang, Z. D.; Xie, S. H.; Zhang, F. Q.; Tu, B.; Yu, C. Z.; Terasaki, O;, Zhao, D. Y. *J. Am. Chem. Soc.* **2004**, *126*, 865.

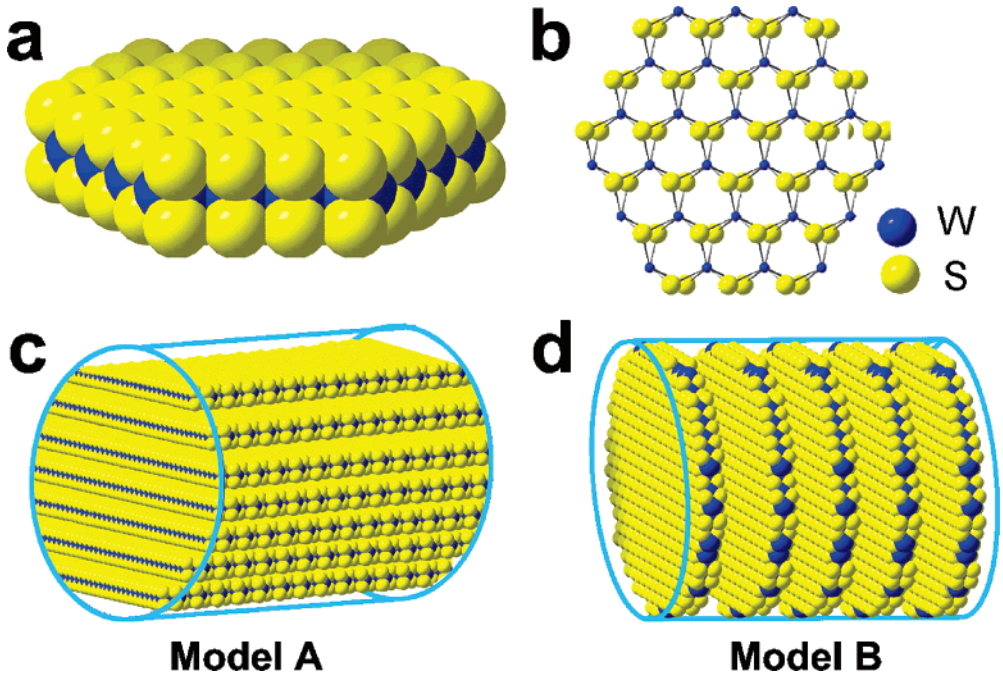

Figure 5. Structure models of the S−W−S trilayer (a, b). Two crystal orientation models: (c) Model A, 2H-WS_2 nanocrystal layers are parallel to the mesochannels, and (d) Model B, 2H-WS_2 nanocrystal layers are perpendicular to the mesochannels.

scale between the crystal lattice and the mesoarrangement.[52,53] Recently, Jiao et al. reported the orientation of Cr_2O_3 replicas casted from mesoporous silica KIT-6 (symmetry of $Ia\bar{3}d$). In some domains, sixfold axes along the [111] direction in the cubic bicontinuous mesostructure were apparently parallel to the [001] axis of Cr_2O_3 particles (rhombohedral, $R3c$).[54−56] By comparison, the oriented growth can be evidenced in each WS_2 particle for the present case. This allows us to study some fundamental issues associated with the correlation of the orientation and the growth for the nanocasted guest materials and the host. WS_2 crystals have a layered structure (Figure 5a and b), which contains a tungsten metal layer sandwiched by two sulfur layers. The bulk crystal is constituted by the stacking of S−W−S trilayers along the *c*-direction in the ABAB fashion. At the edges of each layer, the dangling bonds due to the lack of S or W atoms cause the crystal planes that are parallel to the *c*-axis, high-energy, and quite unstable. The large surface-energy gap that is generated from the crystal planes along different directions can drive the WS_2 layers to roll into nanotubes despite the excess energy from warping.[5,6] As a result, the fewer the edges are, the more thermodynamically stable the crystals are. Two models (Figure 5c and 5d) are established in which the S−W−S trilayers are parallel and perpendicular to the long axis of cylindrical pores. Our simple calculation results (see Supporting Information) demonstrate that the trilayers parallel rather than perpendicular to the pore axis can reduce the unsaturated dangling bonds in the opposite edges. This speculation can explain why the WS_2 crystallites grow following the long axis of the mesochannels. Therefore, the anisotropic nanospace of the mesochannels may be an issue in the surface energies and, in turn, the oriented growth of WS_2 crystallites.

A full filling of the guest molecules inside the nanochannels of the silica hard template is the key issue for nanocasting highly ordered mesoporous replicas. Our results show that 4.27 g of PTA can be incorporated into 1.0 g of SBA-15. These data indicate that the main channels of the mesopores are almost fully filled by guest molecules to the maximum value on the basis of the mesopore volume. XRD and N_2 sorption measurements confirm the complete incorporation of PTA precursors as discussed above. As the tungsten source, PTA molecules have strong hydrogen-bond interactions with the silanol groups on mesoporous silica hard templates. It may favor the incorporation of PTA into the mesochannels. The mesoporous silica SBA-15 is rodlike with particle sizes in the range between 700 and 900 nm, as shown in the SEM image (Figure 6a). After the impregnation, the sulfuration at high temperature, and the subsequent removal of silica by HF, the SEM image shows a minor change (Figure 6b). The reduction of the particle sizes (650−850 nm) is quite small. These results further indicate a true replication with a high yield. The high yield of WS_2 can be attributed to the large volume conversion yield of the PTA precursors to WS_2 crystallites (71 v%, theoretically). The calculation is based on the molecular weight and the density of the reagent $H_3PW_{12}O_{40}\cdot 6H_2O$ (5.53 g/cm^3) and the product WS_2 (7.76 g/cm^3). In other words, 1 cm^3 of PTA precursors can produce about 0.71 cm^3 of WS_2. Therefore, a perfect morphology replication and a high yield are reasonable from the one-step nanocasting. The true replication of the silica scaffold is quite similar to that for mesoporous carbon replicas.[50,57−59] However, it is the volume swelling of carbon owing to the generation of microporosity that causes the true copy in those cases. On the contrary, mesoporous metal oxide replicas could not perfectly replicate the morphology of the mother silica

(52) Yue, B.; Tang, H. L.; Kong, Z. P.; Zhu, K.; Dickinson, C.; Zhou, W. Z.; He, H. Y. *Chem. Phys. Lett.* **2005**, *407*, 83−86.
(53) Zhu, K. K.; Yue, B.; Zhou, W. Z.; He, H. Y. *Chem. Commun.* **2003**, 98−99.
(54) Jiao, K.; Zhang, B.; Yue, B.; Ren, Y.; Liu, S. X.; Yan, S. R.; Dickinson, C.; Zhou, W. Z.; He, H. Y. *Chem. Commun.* **2005**, 5618.
(55) Dickinson, C.; Zhou, W. Z.; Hodgkins, R. P.; Shi, Y. F.; Zhao, D. Y.; He, H. Y. *Chem. Mater.* **2006**, *18*, 3088.
(56) Wang, Y. Q.; Yang, C. M.; Schmidt, W.; Spliethoff, B.; Bill, E.; Schuth, F. *Adv. Mater.* **2005**, *17*, 53−56.

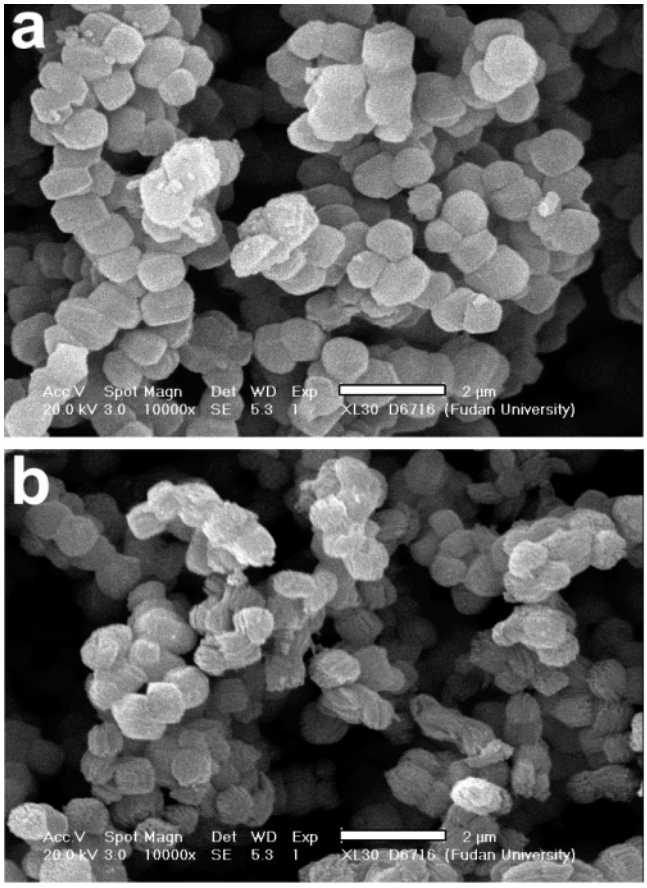

Figure 6. SEM images of mesoporous silica SBA-15 template (a) and mesoporous WS_2-SBA-15 products (b) prepared via the high-temperature (600 °C) reductive sulfuration with H_2S gas followed by the removal of silica by an HF solution. Scale bar is 2 μm.

templates, and the particle sizes were distinctly reduced after the nanocasting process.[42,43,51−55] This can be explained by the low volume conversions from the metal salt precursors to metal oxides (see Supporting Information, Table S1). For example, only 0.085 cm^3 of Co_3O_4 can be yielded from 1 cm^3 of $Co(NO_3)_2{\cdot}6H_2O$, due to the huge mass decrease (from 1.00 g of $Co(NO_3)_2{\cdot}6H_2O$ to 0.28 g of Co_3O_4) and density increase (1.88 g/cm^3 for $Co(NO_3)_2{\cdot}6H_2O$, and 6.07 g/cm^3 for Co_3O_4). This corresponds to an extremely low occupation of the mesochannels (8.5 v% in volume) by Co_3O_4 products after the one-step nanocasting. The same issue is also true for the cases of metal sulfides. A 0.24 cm^3 volume of CdS is produced from 1 cm^3 of $Cd(NO_3)_2{\cdot}4H_2O$. Presumably, W or Mo nitrate salts would be less effective than the polyoxometalates due to the density difference between the precursor and the product sulfide. Therefore, choosing an appropriate precursor is essential in the nanocasting strategy.

The influence of the sulfuration temperature on the final products was also investigated by wide-angle XRD patterns (Figure 7). If the reaction temperature is below 300 °C, no crystalline WS_2 can be found and PTA is partially reserved. The XRD pattern of the composite sulfurated at 400 °C shows

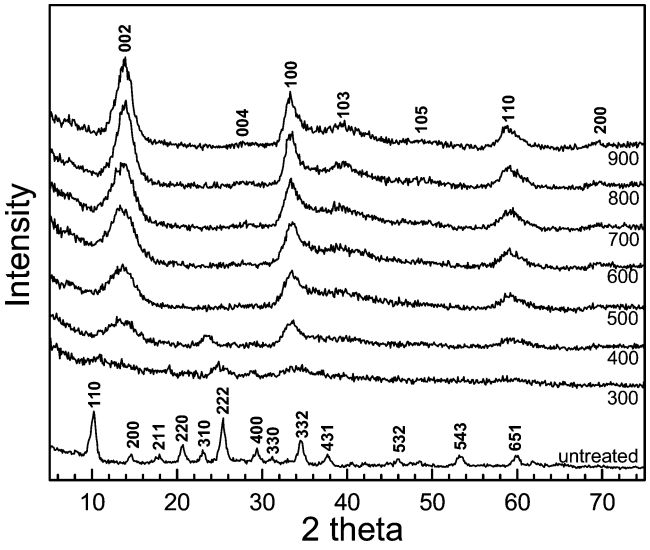

Figure 7. Wide-angle XRD patterns of the mesostructured PTA@SBA-15 composite sulfurated at different temperatures.

three weak and broad diffraction peaks at 2θ values of about 14°, 34°, and 60°, indicating that sulfuration occurs and crystalline WS_2 is formed. However, a diffraction peak at a 2θ value of 23.5° implies the presence of tungsten oxides and incomplete sulfuration. A further increase of temperature to 500 °C results in no phase other than 2H-WS_2, indicating full sulfuration. With increasing reaction temperature, the wide-angle XRD patterns become more resolved and the diffractions get stronger and narrower (Figure 8). These phenomena indicate that the PTA precursors have been entirely sulfurated and the crystallinity is improved upon high-temperature treatment. Consequently, the high-temperature (above 500 °C) sulfuration is another key factor for the successful synthesis of mesoporous WS_2 crystals. The flow rate of H_2S and the reaction time show little influence on the sulfuration. The plenteous sulfur source (three times more than the theoretical quantity) and the long enough reaction time (5 h) are typically adopted.

One distinct advantage of the hard templating approach is that the mesostructures can be easily tuned by varying the mother structure. Here, mesoporous silica KIT-6 was used as the hard template. The XRD pattern reveals that KIT-6 prepared under hydrothermal treatment at 130 °C has a highly ordered cubic bicontinuous ($Ia\bar{3}d$) mesostructure with an a_0 of 22.8 nm (Figure 8a). Upon nanocasting, i.e., the impregnation with PTA, the sulfuration by H_2S, and the elimination of silica with HF solution, the resultants exhibit a well-resolved XRD pattern, similar to that of the mother template (Figure 8a). It manifests that the WS_2 replicas have highly ordered cubic bicontinuous ($Ia\bar{3}d$) mesostructures. The cell parameter is 21.3 nm, indicating a shrinkage of the domain size of 6.6%. This value is analogous to the SBA-15-derived WS_2 crystallites. It is suggested that the structural shrinkage for WS_2 casted from the mesoporous silica scaffold is considerably small, regardless of the mother mesostructure. The wide-angle XRD pattern (Figure 8b) shows that the replicas are composed of nanocrystalline WS_2. N_2 sorption isotherms exhibit type-IV curves with a distinct capillary condensation step for typical mesoporous materials (Figure S3). Crystalline WS_2 replicas obviously have uniform mesopores with a narrow pore size distribution. The BET surface area, mean

(57) Kim, T. W.; Ryoo, R.; Gierszal, K. P.; Jaroniec, M.; Solovyov, L. A.; Sakamoto, Y.; Terasaki, O. *J. Mater. Chem.* **2005**, *15*, 1560.
(58) Tian, B. Z.; Che, S. A.; Liu, Z.; Liu, X. Y.; Fan, W. B.; Tatsumi, T.; Terasaki, O.; Zhao, D. Y. *Chem. Commun.* **2003**, 2726.
(59) Lu, A. H.; Kiefer, A.; Schmidt, W.; Schuth, F. *Chem. Mater.* **2004**, *16*, 100−103.

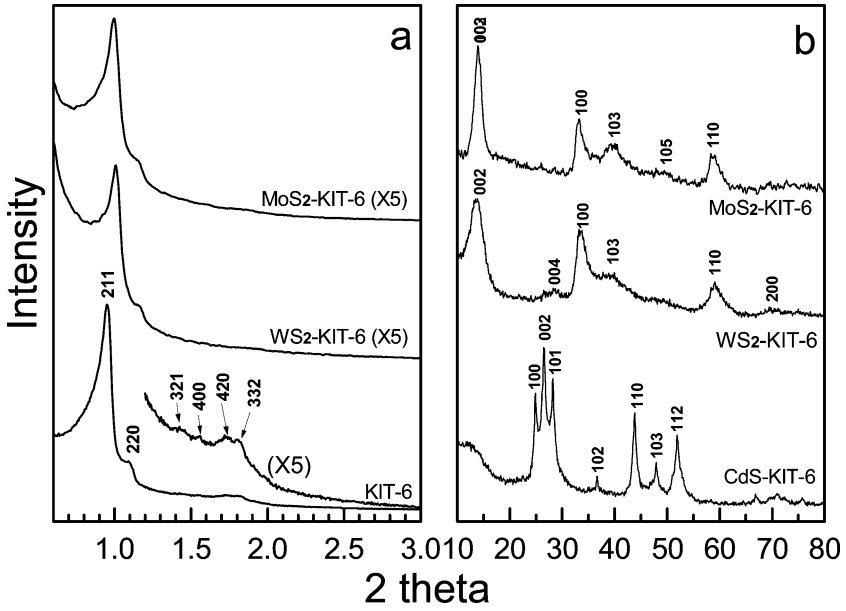

Figure 8. Small-angle (a) and wide-angle (b) XRD patterns of the mesoporous silica KIT-6 template and the mesoporous WS_2-KIT-6, MoS_2-KIT-6, and CdS-KIT-6 replicas.

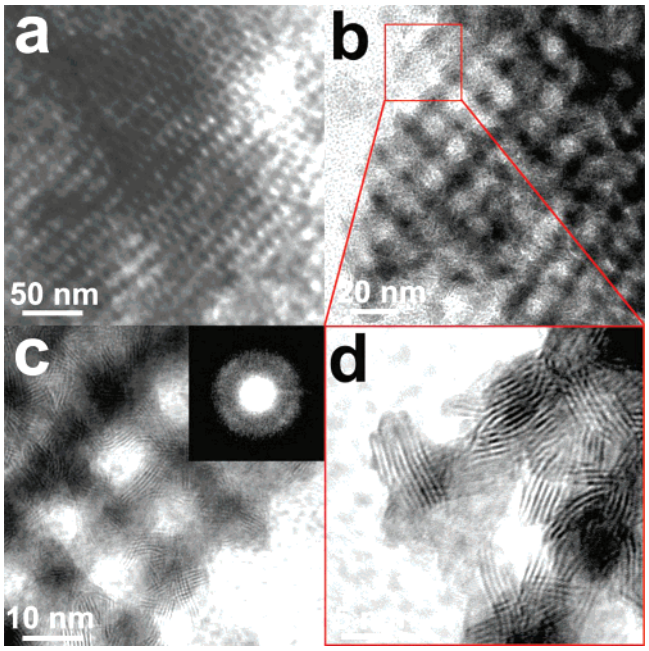

Figure 9. TEM images of cubic mesoporous WS_2 replicated from the KIT-6 hard template with the *Ia*3*d* symmetry along the [331] (a) and [100] (b, c, and d) directions. Inset (c) is corresponding SAED pattern.

pore size, and pore volume are 120 m^2/g, 5.0 nm, and 0.17 cm^3/g, respectively (Table 1).

TEM images further confirm that the mesoporous WS_2 products have a highly ordered 3-D cubic bicontinuous mesostructure (Figure 9). No displaced gyroidal mesostructure (space group of $I4_132$) is observed, owing to the true replication from the KIT-6 mesostructure. The a_0 value estimated from the TEM images is about 20.8 nm, in accordance with that from the XRD pattern. HRTEM images (Figure 9c, d) show that the replicas are composed of nanosized crystalline WS_2 with the layered structure. The orientation of the anisotropic layer structure is not as definite as that for 2-D hexagonally mesostructured WS_2 nanowires. SAED measurements can, however, suggest the partial orientation of the layered crystals (Figure 9c inset). HRTEM images give further evidence on this viewpoint that are recorded from some of the uncoupled enantiomeric gyroidal subframeworks (along the [100] direction) (Figure 9c and d). Like SAB-15 templated WS_2, mesoporous layered WS_2 nanocrystals replicated from KIT-6 are mainly aligned along the mesochannels.

This high-temperature reductive sulfuration method can also be extended to the preparation of mesoporous MoS_2 crystallites with the S−Mo−S sandwiched layered structure by sulfuration of the $H_3PMo_{12}O_{40}\cdot 6H_2O$ precursor inside silica mesochannels. The mesostructure can be tuned by selection of the mother silica template. Mesoporous MoS_2 replicas produced by using the mesoporous silica KIT-6 scaffold exhibit the typical small-angle XRD pattern and TEM images for a highly ordered cubic bicontinuous ($Ia\bar{3}d$) mesostructure (Figure 8a, 10a and b). The cell parameter calculated from the XRD pattern is about 21.7 nm (Table 1). The partial orientation of layered MS_2 nanocrystals can also be observed (Figure 10b, inset). Compared to the crystalline WS_2 replica, mesoporous MoS_2 products (JCPDS: 37-1492) have sharper diffraction peaks in the wide-angle XRD pattern (Figure 8b), indicative of a slightly higher crystallinity. The yield of MoS_2 replicas is also as high as 97 wt % on the basis of the PMA precursor. N_2 sorption measurements (Suppporting Information, Figure S3) show a narrow pore size distribution at a mean value of 4.7 nm, BET surface area of 101 m^2/g, and pore volume of 0.15 cm^3/g (Table 1). Despite a lower density of 5.06 cm^3/g, mesoporous MoS_2 replicas possess lower BET surface areas than WS_2 products with the same mesostructure. This may be related to the higher crystallinity in the former, as shown by the wide-angle XRD patterns (Figure 8b).

An interesting observation is that MoS_2 nanotubes are the products once the loading of the PMA precursor decreases. The preparation of MoS_2 replicas was demonstrated under conditions of a low infilling ratio (1.0 g of PMA precursor to 1.0 g of silica template) and 70-SBA-15 being utilized as a hard template. TEM images (Figure 10c, d, and e) show that relatively uniform multiwalled MoS_2 nanotubes with about 100−300 nm in length,

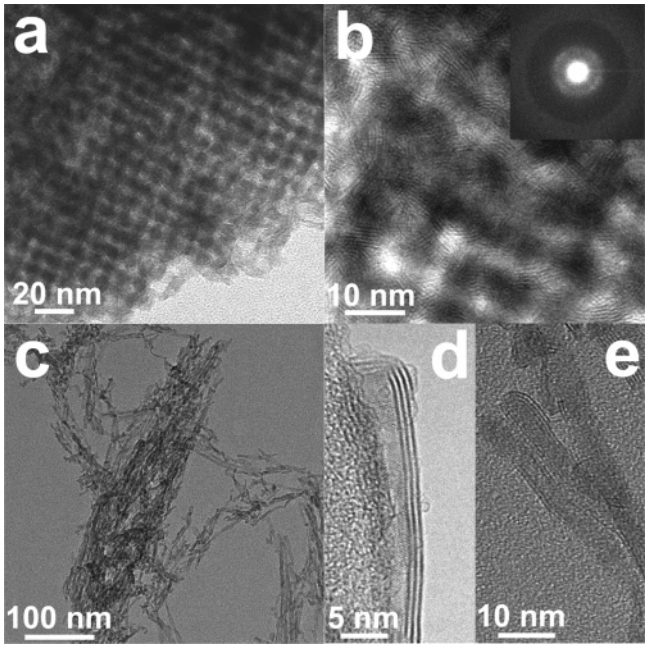

Figure 10. TEM (a) and HRTEM (b) images of mesoporous MoS_2 prepared via high-temperature sulfuration method (600 °C) by using cubic mesoporous silica KIT-6 as a hard template. Inset (b) is the corresponding SAED pattern. TEM (c) and HRTEM images (d and e) of MoS_2 nanotubes replicated under conditions of a low filling amount (1 g PMA/1 g SBA-15) and a hard template of 70-SBA-15.

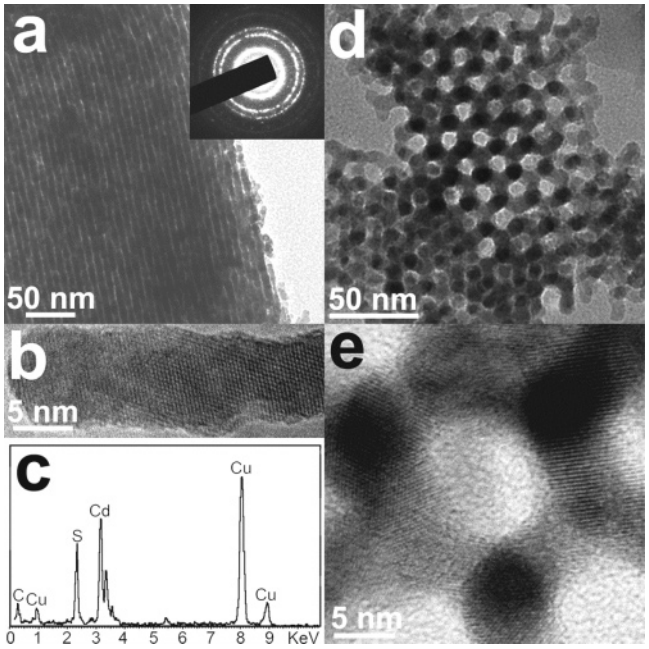

Figure 11. TEM image (a), the corresponding SAED pattern (inset a), HRTEM image (b), and EDX spectrum (c) of mesoporous CdS nanocrystals prepared via high-temperature (300 °C) sulfuration method by using mesoporous silica SBA-15 as a hard template. TEM (d) and HRTEM (e) images of mesoporous CdS nanocrystals replicated from the KIT-6 hard template.

instead of nanorods or nanoparticles, are obtained after etching of the silica template. The nanotubes have 2−3 walls with a closed-end structure (Figure 10d and e). The diameter of the tubes ranges from 5 to 7 nm, close to the diameter of mesochannels, implying a confined effect. To reduce the surface energy, MoS_2 layers would, therefore, roll in the confined mesochannels along the *c*-axis of the SBA-15 mesostructure. This phenomenon has also been observed on mesoporous carbon nanotubes arrays (CMK-5)[60] and metal oxides nanotubes[61−63] casted from SBA-15 mesochannels. The reason may be that the silanol groups on the surface of the mesochannels could interact with the precursors and thus favor the formation of the nanotubes.

This synthesis approach would provide broad and direct access to other mesoporous metal sulfides, and an example given here is cadmium sulfide. Mesoporous CdS replicas can be obtained from the successive steps of the impregnation of $Cd(NO_3)_2{\cdot}4H_2O$ with the SBA-15 template, the high-temperature (300 °C) reductive sulfuration by the H_2S gas, and the removal of the silica template by a NaOH solution (4 M). XRD and TEM measurements reveal that the replicas have an ordered 2-D hexagonal structure (symmetry, *p*6*mm*, Figure 11a). The a_0 value is estimated to be 10.9 nm, close to that of the mother SBA-15 template (Table 1). Strong signals from Cd and S elements were detected by the EDX spectra (Figure 11c). The absence of silicon signals implies the elimination of the silica scaffold. The wide-angle XRD pattern demonstrates that the CdS products are highly crystallized with a main hexagonal wurtzite phase (*P*63*mc*). This result is further confirmed by the SAED measurement (inset Figure 11a). HRTEM images show partial single-crystal features of CdS in some domains (Figure 11b). The yield of the mesoporous CdS replica is 46.8 wt %, based on $Cd(NO_3)_2{\cdot}4H_2O$, distinctly lower than that for WS_2 and MoS_2. The theoretical volume conversion yield of $Cd(NO_3)_2{\cdot}4H_2O$ to CdS is 23.8 υ%, which is quite lower than that for PTA and PMA. The larger mass loss from $Cd(NO_3)_2{\cdot}4H_2O$ to CdS possibly causes the lower yield, and in turn, the obtained mesoporous CdS product has a broader pore size distribution, lower BET surface area of 78 m^2/g, and pore volume of 0.3 cm^3/g. Highly ordered mesoporous CdS with the cubic bicontinuous mesostructure and partial single-crystal characters can also be obtained by using KIT-6 as a hard template (Figure 11d and e).

Conclusions

A general high-temperature reductive sulfuration method has been demonstrated to fabricate highly ordered mesoporous metal sulfides. First, a one-step nanocasting generates metal precursor@mesoporous silica composites. A high-temperature reductive sulfuration is subsequently adopted by using the H_2S gas as a sulfur source to convert the metal precursors to sulfides in the confined nanochannels. After etching silica, mesoporous metal sulfide crystals were obtained as the products. The mesostructure, morphology, compositions, and crystal phase can be tuned by adjustments of the mother template, metal precursors, sulfuration temperature, and the loading amount of the precursors. Mesoporous WS_2 and MoS_2 replicas have been synthesized by using PTA and PMA as precursors. The large volume conversion from the heteropoly acid precursor of PTA (PMA) to WS_2 (MoS_2) and the strong hydrogen interaction

(60) Joo, S. H.; Choi, S. J.; Oh, I.; Kwak, J.; Liu, Z.; Terasaki, O.; Ryoo, R. *Nature* **2001**, *412*, 169.
(61) Ziegler, K. J.; Harrington, P. A.; Ryan, K. M.; Crowley, T.; Holmes, J. D.; Morris, M. A. *J. Phys.: Condens. Matter* **2003**, *15*, 8303.
(62) Sauer, J.; Marlow, F.; Spliethoff, B.; Schuth, F. *Chem. Mater.* **2002**, *14*, 217−224.
(63) Crowley, T. A.; Ziegler, K. J.; Lyons, D. M.; Erts, D.; Olin, H.; Morris, M. A.; Holmes, J. D. *Chem. Mater.* **2003**, *15*, 3518−3522.

between PTA (PMA) and silica mesopore walls are key issues for a true replication of the mother silica template mesostructure with an extremely large yield. High-temperature sulfuration by H_2S at 600 °C transforms the metal precursor to metal sulfides. The frameworks are composed of layered crystalline 2H-WS_2 and 2H-MoS_2 nanowires. The mesostructure can be varied from 2-D hexagonal to 3-D cubic bicontinuous without displacing the gyroidal structure when the mesoporous silica SBA-15 and KIT-6 were used as the hard templates, respectively. Mesoporous WS_2 and MoS_2 replicas have large surfaces areas (up to 120 m^2/g), pore volumes (0.15−0.21 cm^3/g), and narrow pore size distributions (∼4.8 nm). WS_2 and MoS_2 replicas templated from SBA-15 possess a rodlike morphology, and the S−M−S (M = W and Mo) trilayers are partially oriented, parallel to the mesochannels. This orientation can be explained by the confinement of the anisotropic nanochannels as well as the tendency toward the reduction of high-energy layer edges in metal dichalcogenides. When the loading amount of the PMA precursor is low, multiwalled MoS_2 nanotubes with 2−3 walls and 5−7 nm in diameter can be obtained. Other metal sulfide mesostructures such as CdS can also be synthesized. By using $Cd(NO_3)_2{\cdot}4H_2O$ as a precursor, mesoporous CdS nanowires with the partially single-crystal structure can be obtained. Different from that for WS_2 and MoS_2, the yield of CdS replicas is low due to the low volume conversion from $Cd(NO_3)_2{\cdot}4H_2O$ to CdS. Mesoporous CdS replicas thus have a low BET surface area of 85 m^2/g and pore volume of 0.31 cm^3/g. This high-temperature transformation method paves the way for the synthesis of mesoporous CdSe, GaAs, and InP through the simple replacement of H_2S by H_2Se, AsH_3, and PH_3.

Acknowledgment. This work was supported by the NSF of China (20421303, 20407014, 20641001, and 20521140450), the State Key Basic Research Program of the PRC (2006CB202502, 2006CB0N0302), the Shanghai Science & Technology Committee (06DJ14006, 055207078, 05DZ22313), Shanghai Nanotech Promotion Center (0652nm024), Shanghai Education Committee (02SG01,T0402), and the Program for New Century Excellent Talents in Universities (Grant NCET-04-03).

Supporting Information Available: Schematic diagram of the synthesis apparatus; XRD and nitrogen sorption isotherms and pore-size distribution curve of 70-SBA-15; nitrogen sorption isotherms of mesoporous WS_2 and MoS_2 that were prepared from the KIT-6 template; theoretical volume conversion yield of metal salt precursors; calculation process for the comparison of the surface energy between the two crystal orientation models. These materials are available free of charge via the Internet at http://pubs.acs.org.

JA072910N